

Perturbed Coupled-Cluster theory to calculate dipole polarizabilities of closed shell systems: Application to Ar, Kr, Xe and Rn

S. Chattopadhyay,¹ B. K. Mani,² and D. Angom¹

¹*Physical Research Laboratory, Ahmedabad - 380009, Gujarat, India*

²*Department of Physics, University of South Florida, Tampa, Florida 33620, USA*

We use perturbed relativistic coupled-cluster (PRCC) theory to calculate the electric dipole polarizability of noble gas atoms Ar, Kr, Xe and Rn. We also provide a detailed description of the nonlinear terms in the PRCC theory and consider the Dirac-Coulomb-Breit atomic Hamiltonian for the calculations. We find that the largest contribution from Breit interaction to the electric dipole polarizability is 0.1%, in the case of Rn. As we go from Ar to Rn, based on the pattern in the random phase approximation effects, the contraction of the outermost $p_{1/2}$ due to relativistic corrections is discernible without any ambiguity.

PACS numbers: 31.15.bw, 31.15.ap, 31.15.A-, 31.15.ve

I. INTRODUCTION

The knowledge of electric dipole polarizability, α , of atoms and ions is required in different areas of physics and chemistry. It is the lowest order linear response property and relevant to a wide range of physical phenomena ranging from the microscopic to the macroscopic properties. To mention a few macroscopic properties, the dielectric constant and refractive index of gas are among the important ones. In the case of microscopic properties, the parity non-conservation in atoms [1], optical atomic clocks [2, 3] and physics with the condensates of dilute atomic gases [4–6] are of current interest. For accurate theoretical calculation of α , a precise treatment of the electron correlation effects is very important. In the past, a wide range of atomic many body theories were used to calculate α . The recent review by mitroy et al [7] gives a detailed overview of the atomic and ionic polarizabilities.

In the present work we use the PRCC theory to calculate the α of the noble gas atoms. It is a theory we have developed to incorporate a perturbation in the conventional relativistic coupled-cluster (RCC) theory. In general, the coupled-cluster theory (CCT) [8, 9] is one of the most elegant many body theory which takes into account the electron correlation to all order. The details of the CCT and different variants are described in a recent review [10]. The theory has been widely used for atomic [11–14], molecular [15], nuclear [16] and condensed matter physics [17] calculations. The PRCC theory is different from the previous RCC based theories in a number of ways. The most important one is the representation of the cluster operators in the PRCC theory is very different and it has the advantage of incorporating multiple perturbations of different ranks in the electronic sector. One basic technical advantage of PRCC is, it does away with the summation over intermediate states in the first order time-independent perturbation theory. In stead, the summation over all the possible intermediate states within the chosen basis set is subsumed in the perturbed cluster amplitudes.

For the calculations we use the no virtual pair Dirac-

Coulomb-Breit Hamiltonian. However, to assess the importance of Breit interaction we also carry out another series of calculations with the no virtual pair Dirac-Coulomb Hamiltonian. We isolate the changes arising from the Breit interaction by comparing the results from the two sets of the calculations. In contrast, till date, majority of the theoretical calculations of α have been done with the Dirac-Coulomb Hamiltonian. We have chosen the noble gas atoms to study as these systems are ideal to test the closed-shell PRCC theory. In previous works, α of the noble gas atoms were calculated in the framework of many body perturbation theory [18], non-relativistic CCSDT [19] and RCC single, double and triple (RCCSDT) excitation approximation [20]. In the later work, using RCCSDT, the third order Douglas-Kroll method [21] was used. It is an alternative of the Foldy-Wouthuysen (FW) transformation and a quasi-relativistic treatment. For the single particle wave functions, we use the kinetically balanced Gaussian type Dirac-Hartree-Fock orbitals. The results from our PRCC theory calculations are in good agreement with the experimental data and consistent with previous calculations.

The paper is organized as follows. In the Section. II, for completeness and easy reference we briefly describe the RCC theory with the Breit interaction. In section. III we introduce the PRCC theory and provide a detailed description of the tensor structure of the PRCC operators. In section. III B we give the analytical structure of the PRCC equations. In section. III C we present a diagrammatic and algebraic description of the the non-linear terms in the PRCC theory. In section. IV we introduce the formal expression of the dipole polarizability and its representation in the PRCC theory. In the subsequent sections we describe the calculational part, and present the results and discussions. We then end with conclusions. All the results presented in this work and related calculations are in atomic units ($\hbar = m_e = e = 4\pi\epsilon_0 = 1$). In this system of units the velocity of light is α^{-1} , the inverse of fine structure constant. For which we use the value of

$\alpha^{-1} = 137.035\,999\,074$ [22].

II. RCC THEORY

For the high- Z atoms and ions, the Dirac-Coulomb-Breit Hamiltonian, denoted by H^{DCB} , is appropriate to include the relativistic effects. However, there are complications associated with the negative energy continuum states of H^{DCB} . These lead to variational collapse and *continuum dissolution* [23]. A formal approach to avoid these complications is to use the no-virtual-pair approximation. In this approximation, for a neutral atom of N electrons [24]

$$H^{\text{DCB}} = \Lambda_{++} \sum_{i=1}^N [c\boldsymbol{\alpha}_i \cdot \mathbf{p}_i + (\beta_i - 1)c^2 - V_N(r_i)] + \sum_{i < j} \left[\frac{1}{r_{ij}} + g^{\text{B}}(r_{ij}) \right] \Lambda_{++}, \quad (1)$$

where $\boldsymbol{\alpha}$ and β are the Dirac matrices, Λ_{++} is an operator which projects to the positive energy solutions and $V_N(r_i)$ is the nuclear potential. Sandwiching the Hamiltonian with Λ_{++} ensures that the effects of the negative energy continuum states are neglected in the calculations. The last two terms, $1/r_{ij}$ and $g^{\text{B}}(r_{ij})$ are the Coulomb and Breit interactions, respectively. The later, Breit interaction, represents the inter-electron magnetic interactions and is given by

$$g^{\text{B}}(r_{12}) = -\frac{1}{2r_{12}} \left[\boldsymbol{\alpha}_1 \cdot \boldsymbol{\alpha}_2 + \frac{(\boldsymbol{\alpha}_1 \cdot \mathbf{r}_{12})(\boldsymbol{\alpha}_2 \cdot \mathbf{r}_{12})}{r_{12}^2} \right]. \quad (2)$$

The Hamiltonian satisfies the eigen-value equation

$$H^{\text{DCB}}|\Psi_i\rangle = E_i|\Psi_i\rangle, \quad (3)$$

where, $|\Psi_i\rangle$ is the exact atomic state and E_i is the energy of the atomic state. In CCT the exact atomic state is given by the ansatz

$$|\Psi_i\rangle = e^{T^{(0)}}|\Phi_i\rangle, \quad (4)$$

where $|\Phi_i\rangle$ is the reference state wave-function and $T^{(0)}$ is the unperturbed cluster operator. In case of closed-shell atom the model space of the ground state consist of a single Slater determinant, $|\Phi_0\rangle$. For an N -electron closed-shell atom $T^{(0)} = \sum_{i=1}^N T_i^{(0)}$, where i is the order of excitation. In the coupled-cluster single and double (CCSD) excitation approximation,

$$T^{(0)} = T_1^{(0)} + T_2^{(0)}. \quad (5)$$

The CCSD is a good starting point for structure and properties calculations of closed-shell atoms and ions. In the second quantized representation

$$T_1^{(0)} = \sum_{a,p} t_a^p a_p^\dagger a_a, \quad (6a)$$

$$T_2^{(0)} = \frac{1}{2!} \sum_{a,b,p,q} t_{ab}^{pq} a_p^\dagger a_q^\dagger a_b a_a, \quad (6b)$$

where t_{ij} are cluster amplitudes, a_i^\dagger (a_i) are single particle creation (annihilation) operators and $abc\dots$ ($pqr\dots$) represent core (virtual) single particle states or orbitals. The eigenvalue equation of the closed-shell ground state in CCT is

$$H^{\text{DCB}} e^{T^{(0)}}|\Phi_i\rangle = E_0 e^{T^{(0)}}|\Phi_i\rangle. \quad (7)$$

Following similar procedure, the CC eigenvalue equation of closed-shell excited states may be defined as well.

III. PRCC THEORY

To incorporate an additional interaction Hamiltonian H_{int} perturbatively, we introduce the perturbed coupled-cluster operator $\mathbf{T}^{(1)}$. This means, H_{int} is applied once and residual Coulomb interaction to all order in all possible sequences. In general, $\mathbf{T}^{(1)}$ is a tensor operator and the multipole structure depends on the properties of H_{int} . The properties and values of $\mathbf{T}^{(1)}$ indicate the effect of H_{int} to the atomic state. With the perturbation, the modified eigenvalue equation is

$$(H^{\text{DCB}} + \lambda H_{\text{int}})|\tilde{\Psi}_i\rangle = \tilde{E}|\tilde{\Psi}_i\rangle, \quad (8)$$

where λ is the perturbation parameter. Consider the case where H_{int} represents the interaction with an external static electric field \mathbf{E} . The interaction Hamiltonian is then $H_{\text{int}} = -\sum_i \mathbf{r}_i \cdot \mathbf{E} = \mathbf{D} \cdot \mathbf{E}$, where \mathbf{D} is the many electron electric dipole operator. The perturbed atomic state in PRCC theory is

$$|\tilde{\Psi}_i\rangle = e^{T^{(0)} + \lambda \mathbf{T}^{(1)} \cdot \mathbf{E}}|\Phi_i\rangle = e^{T^{(0)}} \left[1 + \lambda \mathbf{T}^{(1)} \cdot \mathbf{E} \right] |\Phi_i\rangle \quad (9)$$

This approach has the advantage of taking into account the effect of multiple perturbations systematically. Other than \mathbf{E} , H_{int} could be one of the interactions internal to the atom like Breit interaction, hyperfine interaction, etc. For the present work, we examine $\mathbf{T}^{(1)}$ arising from \mathbf{E} which is parity odd and vector in the electronic space.

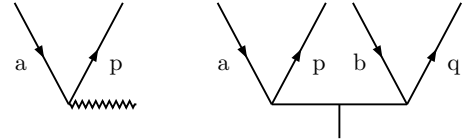


FIG. 1. Diagrammatic representation of $\mathbf{T}_1^{(1)}$ and $\mathbf{T}_2^{(1)}$.

A. Tensor structure of PRCC operator

For the present case, \mathbf{E} as the perturbation, we can write the perturbed single excitation cluster operator as

$$\mathbf{T}_1^{(1)} = \sum_{a,p} \tau_a^p \mathbf{C}_1(\hat{r}) a_p^\dagger a_a. \quad (10)$$

Note that $\mathbf{T}_1^{(1)}$ is a vector operator in the electronic space and the \mathbf{C} -tensor $\mathbf{C}_1(\hat{r})$ represents the vector nature operator. The key difference of $\mathbf{T}_1^{(1)}$ from $T_1^{(0)}$ is $l_a + l_p$ must be odd, in other words $(-1)^{l_a+l_p} = -1$. Here, l_a (l_p) is the orbital angular momentum of the core (virtual) orbital a (p). Diagrammatically, the $\mathbf{T}_1^{(1)}$ operator is represented as shown in Fig. 1(a). It is similar to the conventional representation of $T_1^{(0)}$ but the interaction line is replaced by a wavy line.

The tensor structure of $\mathbf{T}_2^{(1)}$, on the other hand, has additional complications as it consists of two vertices. After due consideration of the H_{int} and $T^{(0)}$ multipole structure, it is represented as

$$\mathbf{T}_2^{(1)} = \sum_{a,b,p,q} \sum_{l,k} \tau_{ab}^{pq}(l,k) \{ \mathbf{C}_l(\hat{r}_1) \mathbf{C}_k(\hat{r}_2) \}^1 a_p^\dagger a_q^\dagger a_b a_a. \quad (11)$$

Like in $\mathbf{T}_1^{(1)}$, \mathbf{C}_k are the \mathbf{C} -tensor operators. Here, two \mathbf{C} -tensor operators of rank l and k are coupled to a rank one tensor operator, $\mathbf{T}_2^{(1)}$. At the two vertices, the orbital angular momenta must satisfy the triangular conditions $|j_a - j_p| \leq l \leq (j_a + j_p)$ and $|j_b - j_q| \leq k \leq (j_b + j_q)$. In addition, the two tensor operators must be such that $|l - k| \leq 1 \leq (l + k)$. These selection rules arise from the triangular conditions at the vertices. The other selection rule follows from the parity condition. For the present case as H_{int} is parity odd $(-1)^{(l_a+l_p)} = -(-1)^{(l_b+l_q)}$. Only then the matrix element $\langle pq | \mathbf{T}_2^{(1)} | ab \rangle$ is nonzero. More details on the first principle analysis of the tensor structure, based on many-body perturbation theory, is given in Ref. [25]. The diagrammatic representation of $\mathbf{T}_2^{(0)}$ is as shown in Fig. 1(b), where the vertical line on the interaction line is to represent the rank of the operator. Further more, this representation, at a later stage, simplifies the angular integration using diagrams.

B. PRCC equations

The eigenvalue equation with the perturbed Hamiltonian is

$$(H^{\text{DCB}} + \lambda H_{\text{int}}) e^{[T^{(0)} + \lambda \mathbf{T}^{(1)} \cdot \mathbf{E}]} |\Phi_0\rangle = \tilde{E}_0 e^{[T^{(0)} + \lambda \mathbf{T}^{(1)} \cdot \mathbf{E}]} |\Phi_0\rangle. \quad (12)$$

When H_{int} is parity odd, like in the present case, there is no first order perturbative correction to energy $\tilde{E}_0 = E_0$. In the CCSD approximation we define the perturbed cluster operator $\mathbf{T}^{(1)}$ as

$$\mathbf{T}^{(1)} = \mathbf{T}_1^{(1)} + \mathbf{T}_2^{(1)}. \quad (13)$$

Using this, the PRCC equations are derived from Eq. (12). The derivation involves several operator contractions and these are more transparent with the normal ordered Hamiltonian $H_N^{\text{DCB}} = H^{\text{DCB}} - \langle \Phi_i | H^{\text{DCB}} | \Phi_i \rangle$. The eigenvalue equation then assumes the form

$$[H_N^{\text{DCB}} + \lambda H_{\text{int}}] |\tilde{\Psi}_0\rangle = [E_0 - \langle \Phi_0 | H^{\text{DCB}} | \Phi_0 \rangle] |\tilde{\Psi}_0\rangle. \quad (14)$$

A more convenient form of the eigenvalue equation is

$$(H_N^{\text{DCB}} + \lambda H_{\text{int}}) |\tilde{\Psi}_0\rangle = \Delta E_0 |\tilde{\Psi}_0\rangle, \quad (15)$$

where, $\Delta E_0 = E_0 - \langle \Phi_0 | H^{\text{DCB}} | \Phi_0 \rangle$ is the ground state correlation energy. Following the definition in Eq. (13), the PRCC eigen-value equation is

$$(H_N^{\text{DCB}} + \lambda H_{\text{int}}) e^{T^{(0)} + \lambda \mathbf{T}^{(1)} \cdot \mathbf{E}} |\Phi_0\rangle = \Delta E_0 e^{T^{(0)} + \lambda \mathbf{T}^{(1)} \cdot \mathbf{E}} |\Phi_0\rangle. \quad (16)$$

Applying $e^{-T^{(0)}}$ from the left, we get

$$[\bar{H}_N^{\text{DCB}} + \lambda \bar{H}_{\text{int}}] e^{\lambda \mathbf{T}^{(1)} \cdot \mathbf{E}} |\Phi_0\rangle = \Delta E_0 e^{\lambda \mathbf{T}^{(1)} \cdot \mathbf{E}} |\Phi_0\rangle, \quad (17)$$

where $\bar{H}_N^{\text{DCB}} = e^{-T^{(0)}} H_N^{\text{DCB}} e^{T^{(0)}}$ is the similarity transformed Hamiltonian. Using the Campbell-Baker-Hausdorff expansion

$$\begin{aligned} \bar{H}^{\text{DCB}} &= H^{\text{DCB}} + [H^{\text{DCB}}, T^{(0)}] + \frac{1}{2!} [[H^{\text{DCB}}, T^{(0)}], T^{(0)}] + \frac{1}{3!} [[[[H^{\text{DCB}}, T^{(0)}], T^{(0)}], T^{(0)}] \\ &\quad + \frac{1}{4!} [[[[[H^{\text{DCB}}, T^{(0)}], T^{(0)}], T^{(0)}], T^{(0)}], T^{(0)}]. \end{aligned} \quad (18)$$

The commutations represent contractions and as H^{DCB} consist of one- and two-body interactions, the expansion terminates at the fourth order. Multiply Eq. (17) from left by $e^{-\lambda \mathbf{T}^{(1)}}$ and consider terms linear in λ , we get the PRCC equation

$$[\bar{H}_N^{\text{DCB}}, \mathbf{T}^{(1)}] \cdot \mathbf{E} + \bar{H}_{\text{int}} |\Phi_0\rangle = 0. \quad (19)$$

Here, the similarity transformed interaction Hamiltonian \bar{H}_{int} terminates at second order as H_{int} is a one-body

interaction Hamiltonian.

Expanding \bar{H}_N^{DCB} and \bar{H}_{int} , the PRCC equation assumes the form

$$\begin{aligned} & \left([H_N^{\text{DCB}}, \mathbf{T}^{(1)}] + \dots \right) \cdot \mathbf{E} |\Phi_0\rangle = \left(\mathbf{D} \right. \\ & \quad \left. + [\mathbf{D}, T^{(0)}] + \frac{1}{2} [[\mathbf{D}, T^{(0)}], T^{(0)}] \right) \cdot \mathbf{E} |\Phi_0\rangle. \end{aligned} \quad (20)$$

Here after, for simplicity, we drop \mathbf{E} from the equations and for compact notation, we use H_N to denote H_N^{DCB} .

The cluster equations of $\mathbf{T}_1^{(1)}$ are obtained after projecting the equation on singly excited states $\langle \Phi_a^p |$. These excitation states, however, must be opposite in parity to

$|\Phi_0\rangle$. The $\mathbf{T}_2^{(1)}$ equations are obtained in a similar way after projecting on the doubly excited states $\langle \Phi_{ab}^{pq} |$. After the application of Wick's theorem, the cluster equations are

$$\langle \Phi_a^p | \left[H_N + \overline{H_N T^{(1)}} + \overline{H_N T^{(0)} T^{(1)}} + \frac{1}{2!} \overline{H_N T^{(0)} T^{(0)} T^{(1)}} \right] | \Phi_0 \rangle = \langle \Phi_a^p | \left[\overline{DT^{(0)}} + \frac{1}{2!} \overline{DT^{(0)} T^{(0)}} \right] | \Phi_0 \rangle, \quad (21)$$

$$\langle \Phi_{ab}^{pq} | \left[H_N + \overline{H_N T^{(1)}} + \overline{H_N T^{(0)} T^{(1)}} + \frac{1}{2!} \overline{H_N T^{(0)} T^{(0)} T^{(1)}} + \dots \right] | \Phi_0 \rangle = \langle \Phi_{ab}^{pq} | \left[\overline{DT^{(0)}} + \frac{1}{2!} \overline{DT^{(0)} T^{(0)}} \right] | \Phi_0 \rangle. \quad (22)$$

Where \overline{AB} represents all possible contractions between the two operators A and B . The Eq. (21) and (22) form a set of coupled nonlinear algebraic equations. However, $T^{(0)}$ are solved first as these are independent of $\mathbf{T}^{(1)}$, the PRCC equations are then reduced to coupled linear algebraic equations. An approximation which incorporates all the important many-body effects like random phase approximation (RPA) is the linearized PRCC (LPRCC). In this approximation, only the terms linear in T , equivalent to retaining only $\overline{H_N T^{(1)}}$ and $\overline{r_i T^{(0)}}$ in Eq. (21) and (22), are considered in the equations. Here after we use T as the general representation of the both $T^{(0)}$ and $\mathbf{T}^{(1)}$ operators.

C. Nonlinear terms in PRCC

The calculations with the LPRCC approximation involves few many-body diagrams, and it is computationally less complex and hence faster. In our calculations, the LPRCC equations are solved first and we use the solutions as the initial guess to solve the PRCC equations. To describe the PRCC equations in detail, we examine each of the nonlinear terms. To begin with consider the second term on the left hand side of Eq. (21) and (22), second order in T , in CCSD approximation it expands to

$$\begin{aligned} \overline{H_N T^{(0)} T^{(1)}} &= \overline{H_N T_1^{(0)} T_1^{(1)}} + \overline{H_N T_1^{(0)} T_2^{(1)}} \\ &+ \overline{H_N T_2^{(0)} T_1^{(1)}} + \overline{H_N T_2^{(0)} T_2^{(1)}}. \end{aligned} \quad (23)$$

All the terms contribute to both $\mathbf{T}_1^{(1)}$ and $\mathbf{T}_2^{(1)}$. Similarly, the third term on the left hand side of Eq. (21) and (22), third order in cluster amplitude, expands to

$$\begin{aligned} \overline{H_N T^{(0)} T^{(0)} T^{(1)}} &= \overline{H_N T_1^{(0)} T_1^{(0)} T_1^{(1)}} + \overline{H_N T_1^{(0)} T_2^{(0)} T_1^{(1)}} \\ &+ \overline{H_N T_1^{(0)} T_1^{(0)} T_2^{(1)}} + \overline{H_N T_1^{(0)} T_2^{(0)} T_2^{(1)}}. \end{aligned} \quad (24)$$

In this equation, out of the four terms, only the first one contributes to $\mathbf{T}_1^{(1)}$. But, all the terms contribute to the $\mathbf{T}_2^{(1)}$. At the fourth order there is only one term and it contributes to only $\mathbf{T}_2^{(1)}$. The terms on the right hand

side of Eq. (21) and (22) expands to

$$\overline{DT^{(0)}} = \overline{DT_1^{(0)}} + \overline{DT_2^{(0)}}, \quad (25)$$

$$\overline{DT^{(0)} T^{(0)}} = \overline{DT_1^{(0)} T_1^{(0)}} + \overline{DT_1^{(0)} T_2^{(0)}}. \quad (26)$$

Here, $\overline{DT_1^{(0)}}$ and $\overline{DT_1^{(0)} T_2^{(0)}}$ are nonzero only for $\mathbf{T}_1^{(1)}$ and $\mathbf{T}_2^{(1)}$, respectively. Each of the terms, after contraction, generate several topologically unique Goldstone diagrams. At this stage, the diagrammatic treatment is the preferred mode of further analysis and calculation. It simplifies the calculations and is well suited to represent contractions between the operators.

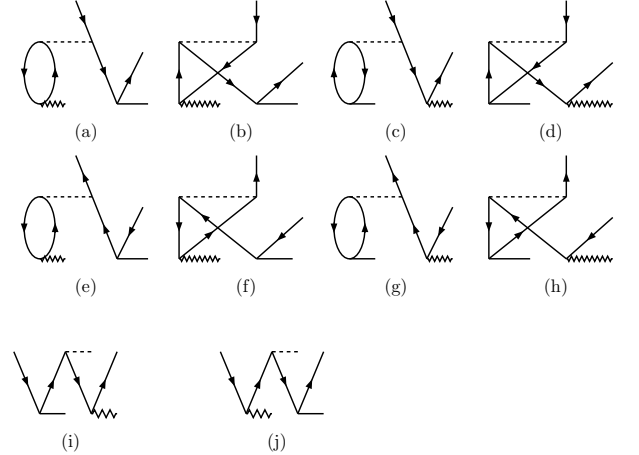


FIG. 2. Diagrams of $\mathbf{T}_1^{(1)}$ arising from $\overline{H_N T_1^{(0)} T_1^{(1)}}$

1. $\mathbf{T}_1^{(1)}$ diagrams

In this section we describe the single excitation diagrams arising from the non linear terms. The many-body diagrams or the Goldstone diagrams are drawn and evaluated as described in ref. [26]. The evaluation of the diagrams consists of calculating the radial and angular integrals. Consider the first term on the right hand side of Eq. (23), $\overline{H_N T_1^{(0)} T_1^{(1)}}$, it is equivalent to ten diagrams

and these are shown in Fig. 2. Algebraically, we can write it as

$$\begin{aligned} \langle \overline{H_N T_1^{(0)}} \mathbf{T}_1^{(1)} \rangle_a^p &= \sum_{bcqa} \tilde{g}_{bcqa} (t_c^p \tau_b^q + t_b^q \tau_c^p) \\ &+ \sum_{bpqr} \tilde{g}_{bpqr} (t_a^r \tau_b^q + t_b^q \tau_a^r), \end{aligned}$$

where $g_{ijkl} = \langle ij | 1/r_{12} + g^B(r_{12}) | kl \rangle$ is the matrix element of the electron-electron interactions and $\tilde{g}_{ijkl} = g_{ijkl} - g_{ijlk}$ is the antisymmetrized matrix element. We have used $\langle \dots \rangle_a^p$ to represent the matrix element $\langle \Phi_a^p | \dots | \Phi_0 \rangle$. The diagrams in Fig. 2(i-j), arising from the one-body part of H_N , evaluate to zero when orbitals are calculated with Dirac-Hartree-Fock potential. The next term, $\overline{H_N T_1^{(0)}} \mathbf{T}_2^{(1)}$, generates eight diagrams and these are shown in Fig. 3. It is to be noted that contractions

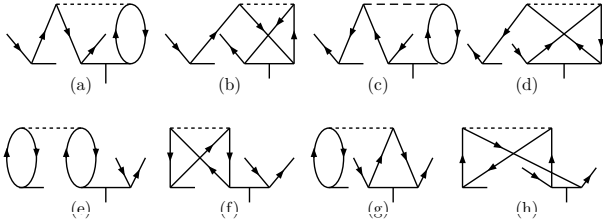


FIG. 3. Diagrams arising from the contraction $\overline{H_N T_1^{(0)}} \mathbf{T}_2^{(1)}$

with only the g_{abpq} type of two-body interaction are non-zero. The algebraic expression of the diagrams is

$$\begin{aligned} \langle \overline{H_N T_1^{(0)}} \mathbf{T}_2^{(1)} \rangle_a^p &= \sum_{bcqr} \tilde{g}_{cbrq} (t_a^r \tau_{pq}^{cb} + t_c^p \tau_{ab}^{rq} + t_c^r \tau_{ba}^{qp} \\ &+ t_b^q \tau_{ac}^{rp}). \end{aligned}$$

At the second order $\overline{H_N T_2^{(0)}} \mathbf{T}_1^{(1)}$ is the last term. Like the previous term, after contraction it generates eight diagrams and these are shown in Fig. 4. The topological

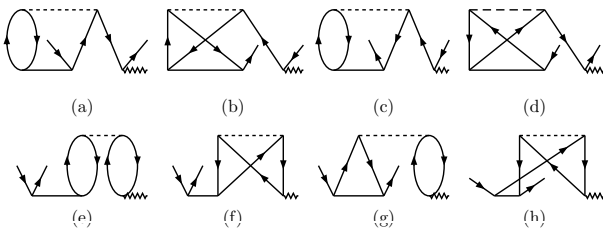


FIG. 4. Diagrams arising from the contraction $\overline{H_N T_2^{(0)}} \mathbf{T}_1^{(1)}$

structure of the diagrams are very similar to those of Fig. 3. The algebraic expression of the diagrams is

$$\begin{aligned} \langle \overline{H_N T_2^{(0)}} \mathbf{T}_1^{(1)} \rangle_a^p &= \sum_{bcqr} \tilde{g}_{bcqr} (t_{ba}^{qr} \tau_p^c + t_{bc}^{qp} \tau_a^r + t_{ab}^{pq} \tau_c^r \\ &+ t_{ac}^{rp} \tau_b^q). \end{aligned}$$

At the third order, as mentioned earlier, only $\overline{H_N T_1^{(0)}} \mathbf{T}_1^{(1)}$ contributes to the $\mathbf{T}_1^{(1)}$ diagrams. This term generate six Goldstone diagrams and these are shown in Fig. 5. The algebraic expression of the dia-

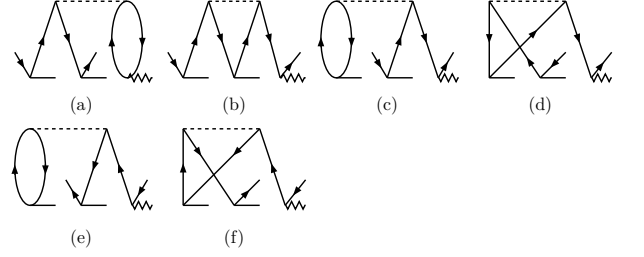


FIG. 5. Diagrams arising from the contraction $\overline{H_N T_1^{(0)}} \mathbf{T}_1^{(1)}$

grams is

$$\begin{aligned} \langle \overline{H_N T_1^{(0)}} \mathbf{T}_1^{(1)} \rangle_a^p &= \sum_{bcqr} \tilde{g}_{bcqr} (t_a^r t_c^p \tau_q^b + t_b^q t_a^r \tau_c^p \\ &+ t_b^q t_c^p \tau_a^r). \end{aligned}$$

In total, the nonlinear terms in the $\mathbf{T}_1^{(1)}$ cluster equation generate thirty Goldstone diagrams. Considering that $T_2^{(0)}$ and $\mathbf{T}_1^{(1)}$ are the dominant cluster operators in the unperturbed RCC and PRCC, respectively, we can expect the magnitude of $\overline{H_N T_2^{(0)}} \mathbf{T}_1^{(1)}$ to be largest.

2. $\mathbf{T}_2^{(1)}$ diagrams

In this section we discuss the Goldstone diagrams of $\mathbf{T}_2^{(1)}$ arising from the non-linear terms on the left hand side of Eq. (22). Consider the second order term, after expansion there are four terms as given in Eq. (23) and all have nonzero contribution to $\mathbf{T}_2^{(1)}$. The first term,

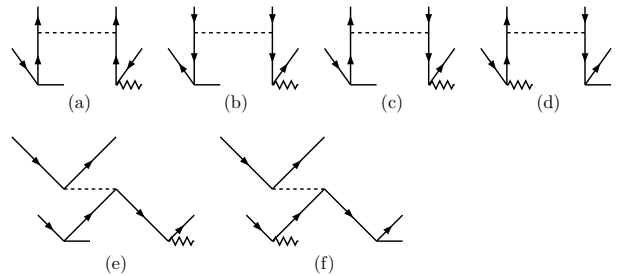


FIG. 6. Diagrams arising from the contraction $\overline{H_N T_1^{(0)}} \mathbf{T}_1^{(1)}$

$\overline{H_N T_1^{(0)}} \mathbf{T}_1^{(1)}$, has six diagrams and these are shown in Fig. 6. The equivalent algebraic expression is

$$\begin{aligned} \langle \overline{H_N T_1^{(0)}} \mathbf{T}_1^{(1)} \rangle_{ab}^{pq} &= \sum_{rs} g_{pqrs} t_a^r \tau_b^s + \sum_{cd} g_{cdab} t_c^p \tau_d^q - \sum_{cr} g_{pcrb} \\ &\times [(t_a^r + t_b^r) \tau_c^q + t_c^q (\tau_a^r + \tau_b^r)], \end{aligned}$$

where, we have used $\langle \dots \rangle_{ab}^{pq}$ to represent the matrix element $\langle \Phi_{ab}^{pq} | \dots | \Phi_0 \rangle$. The next term, $\overline{H_N T_1^{(0)}} \mathbf{T}_2^{(1)}$, has sixteen diagrams and these are shown in Fig. 7. However,

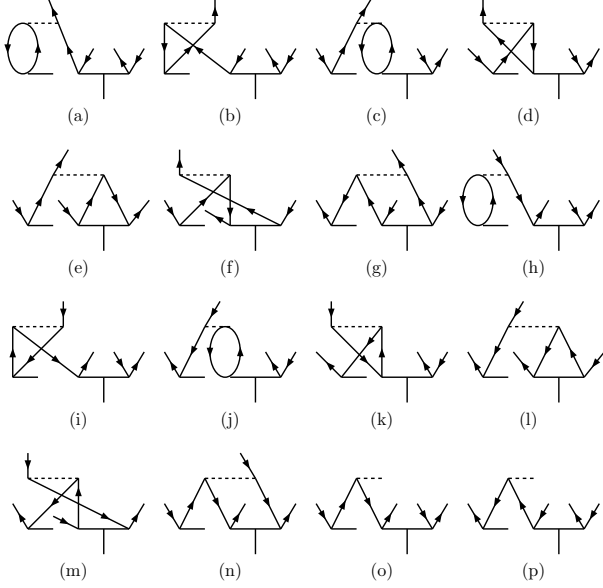


FIG. 7. Diagrams arising from the contraction $\overline{H_N T_1^{(0)}} \mathbf{T}_2^{(1)}$

the last two diagrams are zero when Dirac-Hartree-Fock-Breit orbitals are used, like we do in the present work, in the PRCC calculations. The equivalent algebraic expression is

$$\begin{aligned} \langle \overline{H_N T_1^{(0)}} \mathbf{T}_2^{(1)} \rangle_{ab}^{pq} = & \sum_{crs} g_{cqr s} (t_c^r \tau_{ba}^{sp} - t_c^s \tau_{ba}^{rp} + t_b^s \tilde{\tau}_{ca}^{rp} - t_b^r \tau_{ca}^{sp} \\ & - t_a^r \tau_{cb}^{ps} - t_c^p \tau_{ab}^{rs}) + \sum_{cdr} g_{cdr b} (-t_c^r \tau_{da}^{qp} \\ & + t_d^r \tau_{ca}^{qp} - t_d^q \tilde{\tau}_{ca}^{rp} + t_c^p \tau_{ad}^{rq} + t_a^r \tau_{cd}^{pq}), \end{aligned}$$

where, $\tilde{\tau}_{ca}^{rp} = \tau_{ca}^{rp} - \tau_{ac}^{rp}$ is the antisymmetrised amplitude of $\mathbf{T}_2^{(1)}$. Interchanging the order of excitations of the cluster operators, we get the next term $\overline{H_N T_2^{(0)}} \mathbf{T}_1^{(1)}$. Like in the previous term there are sixteen diagrams and these are shown in Fig. 8 and equivalent algebraic expression is

$$\begin{aligned} \langle \overline{H_N T_2^{(0)}} \mathbf{T}_1^{(1)} \rangle_{ab}^{pq} = & \sum_{crs} g_{cqr s} (\tilde{t}_{ac}^{pr} \tau_b^s - t_{ac}^{ps} \tau_b^r - t_{bc}^{sp} \tau_a^r + t_{ab}^{ps} \tau_c^r \\ & - t_{ab}^{pr} \tau_c^s - t_{ab}^{rs} \tau_c^p) + \sum_{cdr} g_{cdr b} (\tilde{t}_{ca}^{pr} \tau_d^q \\ & - t_{ad}^{pr} \tau_c^q + t_{da}^{qr} \tau_c^p - t_{ad}^{pq} \tau_c^r + t_{ac}^{pq} \tau_d^r \\ & + t_{cd}^{pq} \tau_a^r), \end{aligned}$$

where, $\tilde{t}_{ac}^{pr} = t_{ac}^{pr} - t_{ac}^{rp}$ is the antisymmetrised amplitude of $T_2^{(0)}$. The last second order term is $\overline{H_N T_2^{(0)}} \mathbf{T}_2^{(1)}$ and we can expect a large number of diagrams as both of the cluster operators are double excitation. There are sixteen diagrams and these are shown in Fig. 9. The algebraic

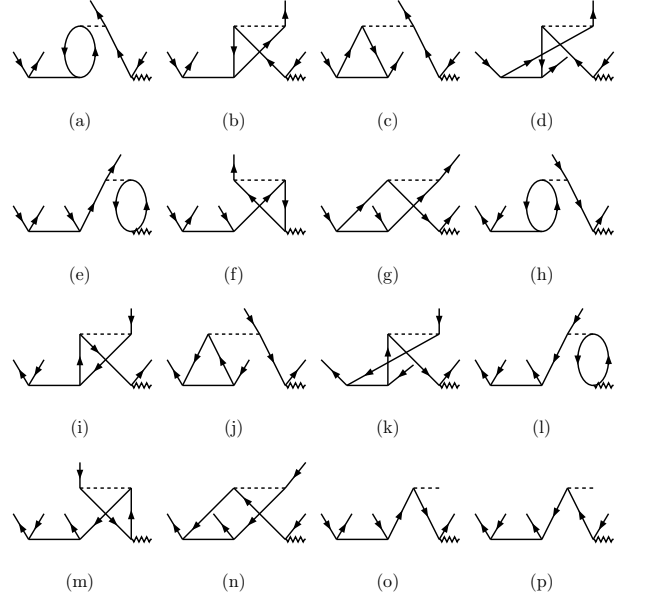


FIG. 8. Diagrams arising from the contraction $\overline{H_N T_2^{(0)}} \mathbf{T}_1^{(1)}$

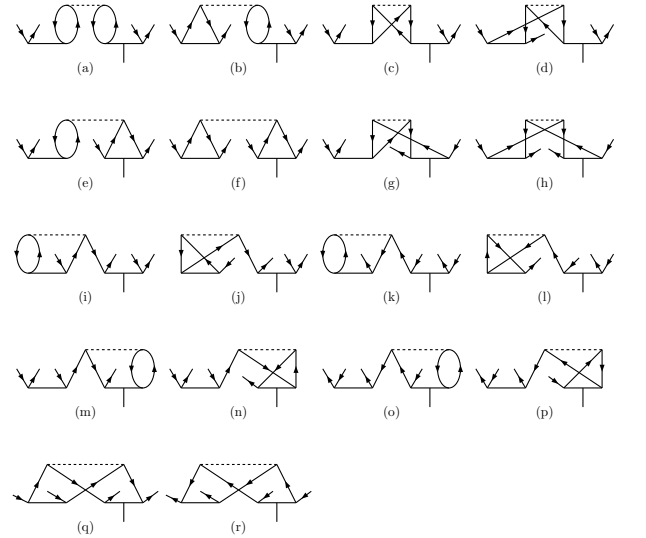


FIG. 9. Diagrams arising from the contraction $\overline{H_N T_2^{(0)}} \mathbf{T}_2^{(1)}$

expression for the diagrams is

$$\begin{aligned} \langle \overline{H_N T_2^{(0)}} \mathbf{T}_2^{(1)} \rangle_{ab}^{pq} = & \sum_{cdrs} g_{cdr s} (\tilde{t}_{ac}^{pr} \tilde{\tau}_{db}^{sq} - \tilde{t}_{ac}^{ps} \tau_{db}^{rq} + t_{ac}^{ps} \tau_{db}^{qr} \\ & + t_{ac}^{sq} \tau_{db}^{pr} - \tilde{t}_{ca}^{rs} \tau_{db}^{pq} - \tilde{t}_{cd}^{rp} \tau_{ab}^{sq} - t_{ab}^{ps} \tau_{dc}^{qr} \\ & + t_{ab}^{pr} \tau_{dc}^{qs} - t_{ac}^{pq} \tilde{\tau}_{bd}^{rs} + t_{ab}^{rs} \tau_{cd}^{pq} + t_{cd}^{pq} \tau_{ab}^{rs}). \end{aligned}$$

Collecting all the diagrams, at the second order, there are 56 Goldstone diagrams in the $\mathbf{T}_2^{(1)}$ equation after contraction of the cluster operators with H_N .

At the third order, all the terms in Eq. (24) have non-zero contributions to $\mathbf{T}_2^{(1)}$. There are six Goldstone diagrams from the first term $\overline{H_N T_1^{(0)}} \mathbf{T}_1^{(0)} \mathbf{T}_1^{(1)}$ and these

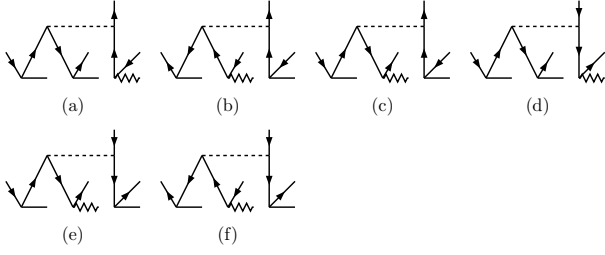


FIG. 10. Diagrams arising from the contraction $\overline{H_N T_1^{(0)} T_1^{(0)} T_1^{(1)}}$

are shown in Fig. 10. The equivalent algebraic expression of the diagrams is

$$\begin{aligned} \langle \overline{H_N T_1^{(0)} T_1^{(0)} T_1^{(1)}} \rangle_{ab}^{pq} = & \sum_{crs} g_{cqr s} [-t_a^r t_c^p \tau_b^s - (t_c^p \tau_a^r - t_a^r \tau_c^p) t_b^s] \\ & + \sum_{cdr} g_{cdr b} [t_a^r (t_c^p \tau_d^q + \tau_c^p t_d^q) + t_c^p \tau_a^r t_d^q]. \end{aligned}$$

The overall contribution from these diagrams is expected to be small as these are quadratic in $T_1^{(0)}$. The next term, $\overline{H_N T_1^{(0)} T_1^{(0)} T_2^{(1)}}$, has ten Goldstone diagrams and these are shown in Fig. 11. The equivalent algebraic expression

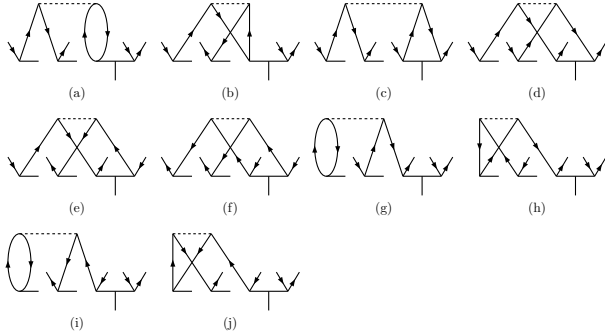


FIG. 11. Diagrams arising from the contraction $\overline{H_N T_1^{(0)} T_1^{(0)} T_2^{(1)}}$

of the diagrams is

$$\begin{aligned} \langle \overline{H_N T_1^{(0)} T_1^{(0)} T_2^{(1)}} \rangle_{ab}^{pq} = & \sum_{cdrs} [t_a^r t_c^p \tilde{\tau}_{bd}^{sq} + t_a^r t_d^p \tau_{cb}^{sq} + t_a^r t_b^s \tau_{cd}^{pq} \\ & + t_d^q (t_a^r \tau_{cb}^{ps} + t_c^p \tau_{ab}^{rs}) - (t_c^r t_a^s - t_c^s t_a^r) \tau_{db}^{pq} \\ & - (t_c^r t_d^p - t_d^r t_c^p) \tau_{ab}^{sq}]. \end{aligned}$$

Contributions from these diagrams will be lower than the previous set as these depend on $T_2^{(1)}$, which is smaller in magnitude than $T_1^{(1)}$, and quadratic in $T_1^{(0)}$ like the previous set. The last third order term, $\overline{H_N T_1^{(0)} T_2^{(0)} T_1^{(1)}}$, has eighteen diagrams and these are shown in Fig. 12. The algebraic equivalent of these diagrams is

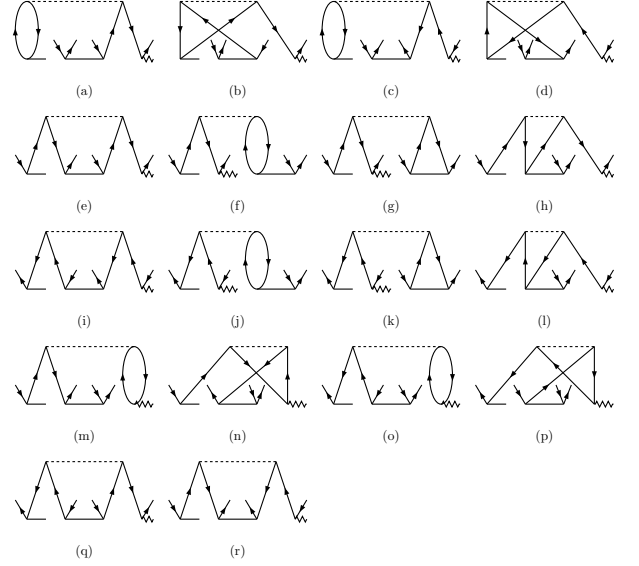


FIG. 12. Diagrams arising from the contraction $\overline{H_N T_1^{(0)} T_2^{(0)} T_1^{(1)}}$

$$\begin{aligned} \langle \overline{H_N T_1^{(0)} T_2^{(0)} T_1^{(1)}} \rangle_{ab}^{pq} = & \sum_{cdrs} [(t_c^s t_{ab}^{pr} - t_c^r t_{ab}^{ps}) \tau_d^q - (t_c^r t_{ad}^{pq} \\ & - t_d^r t_{ac}^{pq}) \tau_b^s + t_a^r (t_{cb}^{ps} \tau_d^q - \tilde{t}_{db}^{sq} \tau_c^p + t_{cb}^{sq} \tau_d^p \\ & - t_{cb}^{pq} \tau_d^s + t_{db}^{pq} \tau_c^s + t_{cd}^{pq} \tau_b^s) + t_c^p (t_{ad}^{rq} \tau_b^s \\ & - \tilde{t}_{db}^{sq} \tau_a^r + t_{db}^{rq} \tau_a^s - t_{ab}^{rq} \tau_d^s + t_{ab}^{sq} \tau_d^r \\ & + t_{ab}^{rs} \tau_d^q)]. \end{aligned}$$

Among the third order terms in the $T_2^{(1)}$ equation this will be the leading term as it depends on $T_2^{(0)}$ and $T_1^{(1)}$, the dominant among the unperturbed and perturbed cluster operators, respectively. There are two Goldstone diagrams from the fourth order term and these are shown in Fig. 13 and the algebraic expression is



FIG. 13. Diagrams arising from the contraction $\overline{H_N T_1^{(0)} T_1^{(0)} T_1^{(0)} T_1^{(1)}}$

$$\langle \overline{H_N T_1^{(0)} T_1^{(0)} T_1^{(0)} T_1^{(1)}} \rangle_{ab}^{pq} = \sum_{cdrs} g_{cdrs} t_a^r t_c^p (t_b^s \tau_d^q + t_d^q \tau_b^s).$$

Among all the diagrams considered so far these two diagrams will have the lowest contributions as these are third order in $T_1^{(0)}$. However, for completeness we include these in the calculations.

3. $\overline{\mathbf{D}}\mathbf{T}^{(0)}$ and $\overline{\mathbf{D}}\mathbf{T}^{(0)}\mathbf{T}^{(0)}$ diagrams

Another group of $\mathbf{T}^{(1)}$ diagrams arise from the contraction of \mathbf{D} and $\mathbf{T}^{(0)}$, which are present on the right hand side of Eq. (21) and (22). In this group, for the $\mathbf{T}_1^{(1)}$ equation there are five Goldstone diagrams and these are shown in Fig. 14. However, among these only the last

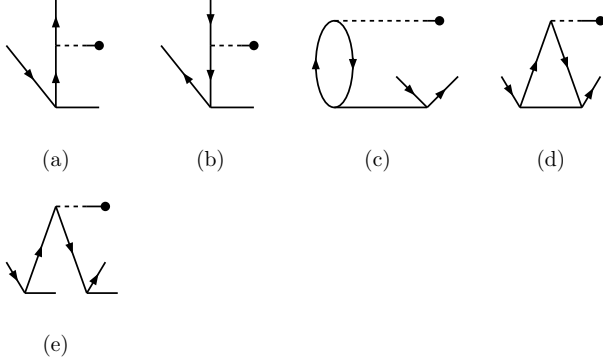


FIG. 14. Singles diagrams arising from the contraction $\overline{H_{\text{int}}}\mathbf{T}^{(0)}$ and $\overline{H_{\text{int}}}\mathbf{T}^{(0)}\mathbf{T}^{(0)}$

one is nonlinear in $\mathbf{T}^{(0)}$. The algebraic expression of the diagrams is

$$\begin{aligned} \langle \overline{\mathbf{D}}\mathbf{T}^{(0)} \rangle_a^p + \langle \overline{\mathbf{D}}\mathbf{T}^{(0)}\mathbf{T}^{(0)} \rangle_a^p &= \sum_q \mathbf{r}_{pq} t_a^q - \sum_c \mathbf{r}_{ca} t_c^p \\ &\quad \sum_{bq} \mathbf{r}_{bq} (t_{ba}^{qp} - t_{ab}^{qp} - t_a^q t_b^q), \end{aligned}$$

where, $\mathbf{r}_{ij} = \langle i|\mathbf{r}|j \rangle$ is the electronic part of the single particle matrix element. For $\mathbf{T}_2^{(1)}$, there are four diagrams and these are shown in Fig. 15 and last two are nonlinear in $\mathbf{T}^{(0)}$. The algebraic expression of the diagrams is

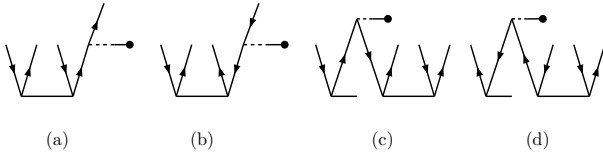


FIG. 15. Doubles diagrams arising from the contraction $\overline{H_{\text{int}}}\mathbf{T}^{(0)}$ and $\overline{H_{\text{int}}}\mathbf{T}^{(0)}\mathbf{T}^{(0)}$

$$\begin{aligned} \langle \overline{\mathbf{D}}\mathbf{T}^{(0)} \rangle_{ab}^{pq} + \langle \overline{\mathbf{D}}\mathbf{T}^{(0)}\mathbf{T}^{(0)} \rangle_{ab}^{pq} &= \sum_r \mathbf{r}_{qr} t_{ab}^{pr} - \sum_c \mathbf{r}_{cb} t_{ac}^{pq} \\ &\quad \sum_{cr} \mathbf{r}_{cr} (-t_a^r t_{cb}^{pq} - t_c^p t_{ab}^{rq}). \end{aligned}$$

This completes the diagrammatic and algebraic analysis of the nonlinear terms in the $\mathbf{T}^{(1)}$ equations. To obtain the linear algebraic equations of the cluster amplitudes, each of the diagrams or terms in the algebraic expression requires further simplification to radial and angular

components. The angular part is evaluated diagrammatically but the diagrams are different from the Goldstone diagrams.

IV. DIPOLE POLARIZABILITY

From the second order time-independent perturbation theory, the ground state dipole polarizability of a closed-shell atom is

$$\alpha = -2 \sum_I \frac{\langle \Psi_0 | \mathbf{D} | \Psi_I \rangle \langle \Psi_I | \mathbf{D} | \psi_0 \rangle}{E_0 - E_I}, \quad (27)$$

where $|\Psi_I\rangle$ are the intermediate atomic states and E_i is the energy of the atomic state. As \mathbf{D} is an odd parity operator, $|\Psi_I\rangle$ must be opposite in parity to $|\Psi_0\rangle$. In the PRCC theory we can write

$$\alpha = - \frac{\langle \tilde{\Psi}_0 | \mathbf{D} | \tilde{\Psi}_0 \rangle}{\langle \tilde{\Psi}_0 | \tilde{\Psi}_0 \rangle}. \quad (28)$$

From the definition of $|\tilde{\Psi}_0\rangle$ in Eq. (9) and based on the parity selection rules, only the terms linear in λ are nonzero. That is,

$$\alpha = - \frac{\langle \Phi_0 | \mathbf{T}^{(1)\dagger} \bar{\mathbf{D}} + \bar{\mathbf{D}} \mathbf{T}^{(1)} | \Phi_0 \rangle}{\langle \Psi_0 | \Psi_0 \rangle}, \quad (29)$$

where, $\bar{\mathbf{D}} = e^{T^{(0)\dagger}} \mathbf{D} e^{T^{(0)}}$, represents the unitary transformed electric dipole operator. Retaining the the leading order terms, we obtain

$$\begin{aligned} \alpha \approx \frac{1}{\mathcal{N}} &\langle \Phi_0 | \mathbf{T}_1^{(1)\dagger} \mathbf{D} + \mathbf{D} \mathbf{T}_1^{(1)} + \mathbf{T}_1^{(1)\dagger} \mathbf{D} \mathbf{T}_1^{(0)} + \mathbf{T}_1^{(0)\dagger} \mathbf{D} \mathbf{T}_1^{(1)} \\ &+ \mathbf{T}_2^{(1)\dagger} \mathbf{D} \mathbf{T}_1^{(0)} + \mathbf{T}_1^{(0)\dagger} \mathbf{D} \mathbf{T}_2^{(1)} + \mathbf{T}_1^{(1)\dagger} \mathbf{D} \mathbf{T}_2^{(0)} \\ &+ \mathbf{T}_2^{(0)\dagger} \mathbf{D} \mathbf{T}_1^{(1)} + \mathbf{T}_2^{(1)\dagger} \mathbf{D} \mathbf{T}_2^{(0)} + \mathbf{T}_2^{(0)\dagger} \mathbf{D} \mathbf{T}_2^{(1)} | \Phi_0 \rangle, \end{aligned} \quad (30)$$

where $\mathcal{N} = \langle \Phi_0 | \exp[T^{(0)\dagger}] \exp[T^{(0)}] | \Phi_0 \rangle$ is the normalization factor, which involves a non-terminating series of contractions between $\mathbf{T}^{(0)\dagger}$ and $\mathbf{T}^{(0)}$. However, in the present work we use $\mathcal{N} \approx \langle \Phi_0 | \mathbf{T}_1^{(0)\dagger} \mathbf{T}_1^{(0)} + \mathbf{T}_2^{(0)\dagger} \mathbf{T}_2^{(0)} | \Phi_0 \rangle$. From the above expression of α , an evident advantage of calculation using PRCC theory is the absence of summation over $|\Psi_I\rangle$. The summation is subsumed in the evaluation of the $\mathbf{T}^{(1)}$ in a natural way. This is one of the key calculational advantage of using PRCC theory.

TABLE I. Comparison between GTO and GRASP92

Atom	GTO	GRASP92
Ar	-528.6837	-528.6837
Kr	-2789.8605	-2788.8605
Xe	-7446.8976	-7446.8976
Rn	-23602.0202	-23602.0232

V. CALCULATIONAL DETAILS

A. Basis set and nuclear density

The first step of our calculations, which is also true of any atomic and molecular calculations, is to generate an orbital basis set. For the present work, we use the Dirac-Hartree-Fock Hamiltonian and even-tempered Gaussian type orbitals (GTOs) [27]. The radial part of the spin-orbitals, the large component in particular, are linear combinations of the Gaussian type functions

$$g_{\kappa p}^L(r) = C_{\kappa i}^L r^{n_{\kappa}} e^{-\alpha_p r^2}, \quad (31)$$

where p is the GTO index and $C_{\kappa i}^L$ is the normalization constant. The exponent α_p depends on two parameters α_0 and β , these are related as $\alpha_p = \alpha_0 \beta^{p-1}$, where $p = 0, 1, \dots, m$ and m is the number of the gaussian type functions. The small components of the spin-orbitals are linear combination of $g_{\kappa p}^S(r)$, which are generated from $g_{\kappa p}^L(r)$ through the kinetic balance condition [28]. We calculate the GTOs on a grid [29] and optimize the values of α_0 and β for individual atoms to match the spin-orbital energies and self consistent field (SCF) energy of GRASP92 [30], which solves Dirac-Hartree-Fock equations numerically. The comparison of the SCF energies are given in Table. I. Except for Rn, there is excellent agreement between the SCF energies obtained from GTO and GRASP92. The symmetry wise values of the optimized α_0 and β are listed in Table. II. To optimize the

TABLE II. The α_0 and β parameters of the even tempered GTO basis used in the present calculations.

Atom	s		p		d	
	α_0	β	α_0	β	α_0	β
Ar	0.00055	1.620	0.00515	2.405	0.00570	2.850
Kr	0.00015	2.015	0.00945	2.975	0.00635	2.845
Xe	0.00012	2.215	0.00495	2.995	0.00745	2.460
Rn	0.00010	2.280	0.00671	2.980	0.00715	2.720

basis set size, we examine the convergence of α using the LPRCC theory. We start with a basis set of 50 GTOs and increase the basis set size in steps through a series of calculations. As an example the results for the case of Kr is listed in Table. III. The value of α changes by only 7×10^{-4} when the number of basis states is increased from 117 to 131. So, we can use the former for our calculations without compromising the desired accuracy.

In the present work we have considered finite size Fermi density distribution of the nucleus

$$\rho_{\text{nuc}}(r) = \frac{\rho_0}{1 + e^{(r-c)/a}}, \quad (32)$$

where, $a = t4\ln(3)$. The parameter c is the half charge radius so that $\rho_{\text{nuc}}(c) = \rho_0/2$ and t is the skin thickness. The PRCC equations are solved iteratively using Jacobi method, we have chosen this method as it is easily parallelizable. The method, however, is slow to converge. So,

TABLE III. Convergence pattern of α (Kr) as a function of the basis set size.

No. of orbitals	Basis size	α
79	(15s, 9p, 9d, 7f, 7g)	16.8759
97	(17s, 11p, 11d, 9f, 9g)	16.7507
117	(21s, 13p, 13d, 11f, 11g)	16.7403
131	(25s, 15p, 14d, 13f, 11g)	16.7396
139	(25s, 16p, 15d, 13f, 13g)	16.7394
155	(29s, 17p, 16d, 15f, 15g)	16.7394

we use direct inversion in the iterated subspace (DIIS) [31] to accelerate the convergence.

B. Breit interaction

There are two different but equivalent approaches, reported in previous works, to calculate the matrix elements of $g^B(r_{12})$. The first approach [32] is to couple the angular part of the orbitals with α to give a linear combination of vector spherical harmonics. This is then combined with the angular part of $1/r_{12}$ for integration. In the second approach [33], $g^B(r_{12})$ is expanded as a linear combination of irreducible tensor operators. In the present work we use the later and employ the expressions given in ref. [34] to incorporate $g^B(r_{12})$ in the GTO and RCC calculations. For GTO calculation [35, 36] provides a very good description to include $g^B(r_{12})$ in finite basis set calculations. To assess the relative importance of Breit interaction, we calculate the first order energy correction

$$\langle H^B \rangle_{\text{DF}} = \langle \Phi_0 | \sum_{i < j} g^B(r_{ij}) | \Phi_0 \rangle, \quad (33)$$

where, $|\Phi_0\rangle$ is the ground state reference function generated from the Dirac-Hartree-Fock spin-orbitals and $H^B = \sum_{i < j} g^B(r_{ij})$ represents the many-particle form of the Breit interaction. The $\langle H^B \rangle_{\text{DF}}$ of the rare gas atoms Ar, Kr, Xe and Rn are listed in Table. IV. For

TABLE IV. SCF Energies for noble gas atoms

Atom	$E_{\text{SCF}}^{\text{DC}}$	$E_{\text{SCF}}^{\text{DCB}}$	$\langle H^B \rangle_{\text{DF}}$	Ref. [37]
Ar	-528.6837	-528.5511	0.1326	0.1324
Kr	-2788.8605	-2787.4310	1.4295	1.4268
Xe	-7446.8976	-7441.1248	5.7728	5.7753
Rn	-23602.0202	-23572.8480	29.1722	29.3968

each atom we calculated the SCF energy with H^{DC} and H^{DCB} , these are $E_{\text{SCF}}^{\text{DC}} = \langle \Phi_0 | H^{\text{DC}} | \Phi_0 \rangle$ and $E_{\text{SCF}}^{\text{DCB}} = \langle \Phi_0 | H^{\text{DCB}} | \Phi_0 \rangle$. Here, $H^{\text{DC}} = H^{\text{DCB}} - H^B$, the atomic Hamiltonian without the Breit interaction. From the table, it is evident that our results are in very good agreement with the previous results [37]. The largest deviation is observed in Rn, our result of $\langle H^B \rangle_{\text{DF}}$ is 0.8% lower than the previous result. However, as the Breit interaction contribution to $E_{\text{SCF}}^{\text{DCB}}$ is a mere 0.12% in Rn,

in absolute terms, the deviation is $\approx 0.001\%$. Our results are also in good agreement with the results of another previous study [38]. In the PRCC calculations, as described earlier, we treat H^B at par with the residual Coulomb interaction. However, to examine the relative importance of Breit interaction, we calculate α with and without H^B .

VI. RESULTS AND DISCUSSIONS

The expression of α in PRCC theory, as mentioned earlier, is a non-terminating series. However, the terms of order higher than quadratic in T have negligible contributions. For this reason, in the present work, we consider upto second order in cluster operator. As mentioned earlier, we have added Breit interaction in the total atomic Hamiltonian, one immediate outcome is, the number of two-electron integrals is larger and storing these, for faster computations, require larger memory. At the first order MBPT, which we use as the initial guess, there is an important change with the inclusion of H^B . With only the Coulomb interaction, at the first order MBPT, the wave operator follows the parity selection rule and only selected multipoles of the Coulomb interaction contributes. However, with H^B , which has opposite parity selection rule compared to Coulomb interaction, all multipoles of the two-electron interaction which satisfy the triangular conditions are allowed. In table V, we list the values of α calculated using the LPRCC theory. For comparison we have also included the results from previous theoretical studies and experimental data. There are no discernible trends in the previous theoretical results and present work. For Kr and Xe, the results from the many-body perturbation theory (MBPT) [18] is higher than the experimental data, but with RCCSD triples (RCCSDT) approximations [20], Ar and Kr have higher values. For Ar our result is 1% higher than the experimental data and this is consistent with the RCCSDT result reported in a previous work. It must, however, be mentioned that the previous work is based on third-order Douglas-Kroll [21] method. Our result for Kr is in excellent agreement with the experimental data. This could be a coincidence arising from well chosen basis set parameters and inherent property of PRCC to incorporate correlation effects more completely within a basis set. In

TABLE V. The static dipole polarizability, α (atomic units), from linearized PRCC and comparison with previous results

Method	Ar	Kr	Xe	Rn
RCCSDT[20]	11.22	16.80	27.06	33.18
CCSDT [19]	11.084	16.839	27.293	34.43
MBPT[18]	11.062	17.214	28.223	
This work	11.213	16.736	26.432	35.391
Expt.[39]	11.091	16.740	27.340	
Expt.[40]	11.081(5)	16.766(8)		

the case of Xe our result is 3.4% lower than the experi-

mental data and 2.4 % lower than the RCCSDT result. The later, difference from the the RCCSDT result, can be partly attributed to the triple excitations. There is no experimental data of α for Rn, the highest Z atom among the noble gases. In ref. [20], the α of Rn is computed using RCCSDT and their result is 6.2% lower than our result.

To estimate the importance of Breit interaction, we exclude H^B in the PRCC calculations and the value after excluding H^B are 11.202, 16.728, 26.404, 35.266 for Ar, Kr, Xe and Rn respectively. These represent a decrease of 0.010, 0.012, 0.021 and 0.133 from the results with the exclusion of H^B . Except for Rn, the change in α is below 0.1%. This implies that to obtain accurate results for Rn, it is desirable to include Breit interaction in the calculations.

TABLE VI. Contribution to α from different terms of the dressed dipole operator in the linearized PRCC theory

Contributions from	Ar	Kr	Xe	Rn
$\mathbf{T}_1^{(1)\dagger}\mathbf{D} + \text{h.c.}$	12.191	18.613	30.855	41.641
$\mathbf{T}_1^{(1)\dagger}\mathbf{D}\mathbf{T}_2^{(0)} + \text{h.c.}$	-0.545	-0.888	-1.677	-2.328
$\mathbf{T}_2^{(1)\dagger}\mathbf{D}\mathbf{T}_2^{(0)} + \text{h.c.}$	0.510	0.748	1.352	1.862
$\mathbf{T}_1^{(1)\dagger}\mathbf{D}\mathbf{T}_1^{(0)} + \text{h.c.}$	-0.057	-0.118	-0.357	-0.301
$\mathbf{T}_2^{(1)\dagger}\mathbf{D}\mathbf{T}_1^{(0)} + \text{h.c.}$	0.022	0.038	0.092	0.073
Normalization	1.081	1.099	1.145	1.157
Total	11.213	16.736	26.432	35.391

To examine the results in more detail, the contributions from the terms in the expression of α given in Eq. (30) are listed in Table VI. It is evident that $\mathbf{T}_1^{(1)\dagger}\mathbf{D}$ and its hermitian conjugate have the leading order contributions. This is to be expected as these terms include the Dirac-Hartree-Fock-Breit contribution and RPA effects, which have the dominant contributions. In all the cases, the result from $\mathbf{T}_1^{(1)\dagger}\mathbf{D}$ is larger than the total value and shows dependence on Z : the results of Ar, Kr, Xe and Rn from this term are 8.7%, 11.2%, 16.7% and 17.7% higher than the total values, respectively. The next to leading order terms are $\mathbf{T}_1^{(1)\dagger}\mathbf{D}\mathbf{T}_2^{(0)}$ and its hermitian conjugate. Contributions from these terms are, approximately, a factor of twenty smaller than the leading order terms and opposite in phase. On closer inspection, it is natural that $\mathbf{T}_1^{(1)\dagger}\mathbf{D}\mathbf{T}_2^{(0)}$ and its hermitian conjugate are the next to leading order terms. Among the second order terms, these are the ones which have $\mathbf{T}_1^{(1)}$ and $\mathbf{T}_2^{(0)}$, the dominant cluster amplitudes in the perturbed and unperturbed relativistic coupled-cluster theories. The results from $\mathbf{T}_1^{(1)\dagger}\mathbf{D}\mathbf{T}_2^{(0)}$ have large cancellations with the term $\mathbf{T}_2^{(1)\dagger}\mathbf{D}\mathbf{T}_2^{(0)}$, which is almost the same in magnitude but opposite in sign. Interestingly, a similar pattern is also observed with the $\mathbf{T}^{(1)\dagger}\mathbf{D}\mathbf{T}_2^{(0)}$ terms. Namely, the results from $\mathbf{T}_1^{(1)\dagger}\mathbf{D}\mathbf{T}_2^{(0)}$ are negative and opposite in sign to $\mathbf{T}_2^{(1)\dagger}\mathbf{D}\mathbf{T}_2^{(0)}$.

TABLE VII. Contribution to α from different terms of the dressed dipole operator in the non-linear PRCC theory

Contributions from	Ar	Kr	Xe
$\mathbf{T}_1^{(1)\dagger}\mathbf{D} + \text{h.c.}$	12.950	18.622	33.108
$\mathbf{T}_1^{(1)\dagger}\mathbf{D}\mathbf{T}_2^{(0)} + \text{h.c.}$	-0.579	-0.899	-1.7964
$\mathbf{T}_2^{(1)\dagger}\mathbf{D}\mathbf{T}_2^{(0)} + \text{h.c.}$	0.488	0.769	1.278
$\mathbf{T}_1^{(1)\dagger}\mathbf{D}\mathbf{T}_1^{(0)} + \text{h.c.}$	-0.061	-0.096	-0.392
$\mathbf{T}_2^{(1)\dagger}\mathbf{D}\mathbf{T}_1^{(0)} + \text{h.c.}$	0.022	0.035	0.095
Normalization	1.081	1.099	1.145
Total	11.859	16.771	28.203

The results from the full PRCC, including the terms nonlinear in cluster amplitudes are given in table VII. From the table, it is clear that the nonlinear terms tend to increase the deviations from the experimental data. A similar trend was reported in our previous work on Ne [41]. For Ar, the non-linear PRCC theory result is 5.4% larger than the result from linearized PRCC and it is 6.5% larger than the experimental result. Similarly, for Xe the nonlinear PRCC result is 6.3% larger than the linearized PRCC result. On the other hand for Kr, the non-linear PRCC results are marginally larger than the linearized PRCC results. The larger values of α in the non-linear PRCC can almost entirely be attributed to higher value of $\mathbf{T}_1^{(1)\dagger}\mathbf{D}$ and it's hermitian conjugate. It means that the non-linear terms tend to increase the RPA effects. This is an example where inclusion of higher order terms enhance the uncertainty. It is possible that triple excitations, higher order excitation not considered in the present work, may balance the deviations and bring the results closer to the experimental data.

TABLE VIII. Core orbital contribution from $\mathbf{T}_1^{(1)\dagger}\mathbf{D}$ to α

Ar	Kr	Xe	Rn
8.152 ($3p_{3/2}$)	12.872 ($4p_{3/2}$)	22.292 ($5p_{3/2}$)	34.524 ($6p_{3/2}$)
3.914 ($3p_{1/2}$)	5.572 ($4p_{1/2}$)	8.120 ($5p_{1/2}$)	6.502 ($6p_{1/2}$)
0.100 ($3s_{1/2}$)	0.058 ($4s_{1/2}$)	0.222 ($4d_{5/2}$)	0.382 ($5d_{5/2}$)
0.012 ($2p_{3/2}$)	0.056 ($3d_{5/2}$)	0.140 ($4d_{3/2}$)	0.214 ($5d_{3/2}$)

For a more detailed analysis of the contributions from the RPA effects, we consider contributions from each of the core orbitals in $\mathbf{T}_1^{(1)\dagger}\mathbf{D}$. In terms of orbital indices the expression is

$$\mathbf{T}_1^{(1)\dagger}\mathbf{D} + \text{H.c.} = \sum_{ap} (\mathbf{d}_{ap}\tau_a^p + \tau_a^{p*}\mathbf{d}_{pa}), \quad (34)$$

where, $\mathbf{d}_{ap} = \langle a|\mathbf{d}|p\rangle$ with \mathbf{d} as the single particle electric dipole operator. The four leading core orbitals (a) for each of the atoms are listed in Table. VIII. In all the cases, the result from the outermost $np_{3/2}$ valence orbitals are the largest. This is not surprising as these are the orbitals which are spatially most extended. In

addition, as the matrix elements in the expression of α has a quadratic dependence on radial distance, orbitals with larger radial extent have higher contributions. The next largest values arise from the $np_{1/2}$ valence orbitals. An interesting pattern is to be noticed in the results, with higher Z the ratio of the contribution from $np_{3/2}$ to $np_{1/2}$ increases. For Ar, Kr and Xe the ratios are 2.1, 2.3 and 2.7, respectively. However, the ratio for Rn is much larger, it is 5.3. The reason for the trend in the ratios is the contraction of the $np_{1/2}$ core orbitals due to relativistic corrections. Hence, the $np_{1/2}$ valence orbitals of higher Z atoms show larger contraction and accounts for the higher ratio. The third largest contributions in Ar and Kr arise from the $3s_{1/2}$ and $4s_{1/2}$ orbitals, respectively. This is expected as these are the orbitals which are energetically just below the np orbitals and spatially as well. Extending the same pattern, for Xe and Rn, the third largest contributions must be from the $5s_{1/2}$ and $6s_{1/2}$ orbitals, respectively, but this is not case. These orbitals are contracted because of relativistic corrections and the diffused $nd_{5/2}$ orbitals have the third largest values. From the trends in the results of the RPA effects, it is obvious that the relativistic corrections are important for Xe and Rn.

TABLE IX. Core orbitals contribution from $\mathbf{T}_1^{(1)\dagger}\mathbf{D}\mathbf{T}_2^{(0)}$ to α of Argon and Krypton

Ar	Kr
-0.124 ($3p_{3/2}, 3p_{1/2}$)	-0.205 ($4p_{3/2}, 4p_{1/2}$)
-0.118 ($3p_{3/2}, 3p_{3/2}$)	-0.193 ($4p_{3/2}, 4p_{3/2}$)
-0.027 ($3p_{1/2}, 3p_{1/2}$)	-0.038 ($4p_{1/2}, 4p_{1/2}$)
-0.006 ($3p_{3/2}, 3s_{1/2}$)	-0.008 ($4p_{3/2}, 3d_{5/2}$)

Next, we examine the pair-correlation effects, which manifest through the next to leading order terms, $\mathbf{T}_1^{(1)\dagger}\mathbf{D}\mathbf{T}_2^{(0)}$ and it's hermitian conjugate. In terms of orbital indices

$$\mathbf{T}_1^{(1)\dagger}\mathbf{D}\mathbf{T}_2^{(0)} + \text{H.c.} = \sum_{abpq} [(\tau_a^{p*}\mathbf{d}_{bq} - \tau_a^q\mathbf{d}_{bp})t_{ab}^{pq} + t_{ab}^{pq*}(\tau_a^p\mathbf{d}_{qb} - \tau_a^q\mathbf{d}_{pb})]. \quad (35)$$

The results of the four leading terms, listed in terms of the pairs of the core orbitals (ab), for Ar and Kr are given in Table. IX. From the table we can identify ($np_{3/2}, np_{1/2}$) as the most dominant pairing of the core-orbitals among the double excitations. Considering that the pairing is between different orbitals, the number of cluster amplitudes is large and this explains the large contribution. The second and third dominant contributions, from the ($np_{3/2}, np_{3/2}$) and ($np_{1/2}, np_{1/2}$) pairs, are also on account of number of cluster amplitudes. Since $np_{3/2}$ and $np_{1/2}$ each accommodate four and two electrons each, respectively, the former has a larger number of cluster amplitudes. There is a small but important change in the results of Xe and Rn listed in Table. X. The

most dominant pair for these atoms is $(np_{3/2}, np_{3/2})$ and $(np_{3/2}, np_{1/2})$ is the second. This is in contrast to the sequence observed in Ar and Kr. The reason is, although the later pair has more cluster amplitudes, the $np_{1/2}$ is contracted due to relativistic corrections. So, the contributions to α from $T_2^{(0)}$ involving $np_{1/2}$ is smaller. The difference between the results from the two pairs is even more dramatic in Rn. There are other changes in the case of Rn. The $(6p_{3/2}, 5d_{5/2})$ pair, involving the diffused $5d_{5/2}$, is now the third largest contribution. And the $(6p_{1/2}, 6p_{1/2})$, which has the contracted $6p_{1/2}$ orbital, is the fourth largest contribution. This difference in the sequence of leading contributions for Rn arises from the larger relativistic corrections.

TABLE X. Core orbitals contribution from $\mathbf{T}_1^{(1)\dagger} \mathbf{D} T_2^{(0)}$ to α of Xenon and Radon

Xe	Rn
-0.361 ($5p_{3/2}, 5p_{3/2}$)	-0.591 ($6p_{3/2}, 6p_{3/2}$)
-0.359 ($5p_{3/2}, 5p_{1/2}$)	-0.387 ($6p_{3/2}, 6p_{1/2}$)
-0.054 ($5p_{1/2}, 5p_{1/2}$)	-0.071 ($6p_{3/2}, 5d_{5/2}$)
-0.035 ($5p_{3/2}, 4d_{5/2}$)	-0.036 ($6p_{1/2}, 6p_{1/2}$)

To estimate the uncertainty in our calculations, we have identified few important sources of uncertainty. The first one is the truncation of orbital basis sets. Although we start with 9 symmetry for all the calculations, we increase the number of symmetries upto 13 in steps. The basis set chosen for the results given are after the value of α converges to 10^{-4} . So, the uncertainty from the basis set truncation is negligible. The second source of uncertainty is the truncation of CC theory at the single and double excitation for both the unperturbed and perturbed RCC theory. Based on earlier studies, the contributions from the triples and quadruple excitations could be at the most $\approx 3.3\%$. This is also consistent with the deviations from the experimental data. Finally, the truncation of $e^{\mathbf{T}^{(1)\dagger}} \mathbf{D} e^{T^{(0)}} + e^{T^{(0)\dagger}} \mathbf{D} e^{\mathbf{T}^{(1)}}$ is another source of uncertainty. From our earlier studies with iterative method [42], to incorporate higher order terms in the properties calculations with CC theory, the contributions from the

third or higher order in is negligibly small. Quantum electrodynamical (QED) corrections in this set of calculations is another source of uncertainty. However, it is expected to be smaller than the correction from the Breit interaction. As the largest Breit correction, in the case of Rn, is 0.1%, we can assume the corrections from QED effects to be at the most 0.1%. So, adding this the maximum uncertainty in our calculations is 3.4%. However, it must be emphasized that, for Ar and Kr, the uncertainty is much smaller than this bound.

VII. CONCLUSION

The PRCC theory is a general extension of the RCC method to incorporate an additional perturbation. The present work demonstrates that it is suitable for properties calculations for closed-shell atoms. Although, in the present work we have used PRCC to calculate electric dipole polarizability, the method can be extended to calculate other atomic properties as well.

From the present study, through the detailed analysis and identification of the dominant contributions, the relativistic correction to α of noble gas atoms arising from the contraction of the outermost $p_{1/2}$ is significant. The notable impact of this is the higher fractional contribution from $np_{3/2}$ in the terms which subsume RPA effects, $\mathbf{T}_1^{(1)\dagger} \mathbf{D}$ and its hermitian conjugate, as we go from Ar to Rn. For Rn, the effect of relativistic corrections is also identifiable without ambiguity in the pair-correlation effects, the $(6p_{1/2}, 6p_{1/2})$ pair is below the $(6p_{3/2}, 5d_{5/2})$ pair for $\mathbf{T}_1^{(1)\dagger} \mathbf{D} T_2^{(0)}$.

We have also examined the importance of Breit interaction in the calculation of α . The largest change of 0.1% is associated with Rn, the heaviest noble gas atom. So, when the required uncertainty of the calculations is below 1%, the inclusion of Breit interaction is desirable for higher Z closed-shell atoms like Rn.

ACKNOWLEDGMENTS

We thank S. Gautam, Arko Roy and Kuldeep Suthar for useful discussions. The results presented in the paper are based on the computations using the 3TFLOP HPC Cluster at Physical Research Laboratory, Ahmedabad.

-
- [1] I. Khriplovich, *Parity Nonconservation in Atomic Phenomena* (Gordon and Breach Science Publishers, Philadelphia, 1991).
 - [2] T. Udem, R. Holzwarth, and T. W. Hansch, *Nature* **416**, 233 (2002).
 - [3] S. A. Diddams, J. C. Bergquist, S. R. Jefferts, and C. W. Oates, *Science* **306**, 1318 (2004).
 - [4] M. H. Anderson, J. R. Ensher, M. R. Matthews, C. E. Wieman, and E. A. Cornell, *Science* **269**, 198 (1995).
 - [5] C. C. Bradley, C. A. Sackett, J. J. Tollett, and R. G. Hulet, *Phys. Rev. Lett.* **75**, 1687 (1995).
 - [6] K. B. Davis, M. O. Mewes, M. R. Andrews, N. J. van Druten, D. S. Durfee, D. M. Kurn, and W. Ketterle, *Phys. Rev. Lett.* **75**, 3969 (1995).
 - [7] J. Mitroy, M. S. Safronova, and C. W. Clark, *J. Phys. B* **43**, 202001 (2010).
 - [8] F. Coester, *Nucl. Phys.* **7**, 421 (1958).
 - [9] F. Coester and H. Kümmel, *Nucl. Phys.* **17**, 477 (1960).
 - [10] R. J. Bartlett and M. Musiał, *Rev. Mod. Phys.* **79**, 291 (2007).

- [11] B. K. Mani, K. V. P. Latha, and D. Angom, Phys. Rev. A **80**, 062505 (2009).
- [12] H. S. Nataraj, B. K. Sahoo, B. P. Das, and D. Mukherjee, Phys. Rev. Lett. **101**, 033002 (2008).
- [13] R. Pal, M. S. Safronova, W. R. Johnson, A. Derevianko, and S. G. Porsev, Phys. Rev. A **75**, 042515 (2007).
- [14] G. Gopakumar, H. Merlitz, S. Majumder, R. K. Chaudhuri, B. P. Das, U. S. Mahapatra, and D. Mukherjee, Phys. Rev. A **64**, 032502 (2001).
- [15] T. A. Isaev, A. N. Petrov, N. S. Mosyagin, A. V. Titov, E. Eliav, and U. Kaldor, Phys. Rev. A **69**, 030501 (2004).
- [16] G. Hagen, T. Papenbrock, D. J. Dean, and M. Hjorth-Jensen, Phys. Rev. Lett. **101**, 092502 (2008).
- [17] R. F. Bishop, P. H. Y. Li, D. J. J. Farnell, and C. E. Campbell, Phys. Rev. B **79**, 174405 (2009).
- [18] A. J. Thakkar, H. Hettema, and P. E. S. Wormer, J. Chem. Phys. **97**, 3252 (1992).
- [19] P. Soldan, E. P. F. Lee, and T. G. Wright, Phys. Chem. Chem. Phys. **3**, 4661 (2001).
- [20] T. Nakajima and K. Hirao, Chem. Lett. **30**, 766 (2001).
- [21] T. Nakajima and K. Hirao, J. Chem. Phys. **113**, 7786 (2000).
- [22] P. J. Mohr, B. N. Taylor, and D. B. Newell, “Codata recommended values of the fundamental physical constants: 2010,” (2012).
- [23] G. E. Brown and D. G. Ravenhall, Proceedings of the Royal Society of London. Series A. Mathematical and Physical Sciences **208**, 552 (1951).
- [24] J. Sucher, Phys. Rev. A **22**, 348 (1980).
- [25] B. K. Mani and D. Angom, ArXiv e-prints (2011), 1105.3447.
- [26] I. Lindgren and J. Morrison, *Atomic Many-Body Theory* (Springer, 2nd Edition, 1986).
- [27] A. K. Mohanty and E. Clementi, J. Chem. Phys. **93**, 1829 (1990).
- [28] R. E. Stanton and S. Havriliak, J. Chem. Phys. **81**, 1910 (1984).
- [29] R. K. Chaudhuri, P. K. Panda, and B. P. Das, Phys. Rev. A **59**, 1187 (1999).
- [30] F. A. Parpia, C. Froese Fischer, and I. P. Grant, Comp. Phys. Comm. **94**, 249 (1996).
- [31] P. Pulay, Chem. Phys. Lett. **73**, 393 (1980).
- [32] J. B. Mann and W. R. Johnson, Phys. Rev. A **4**, 41 (1971).
- [33] I. P. Grant and N. C. Pyper, J. Phys. B **9**, 761 (1976).
- [34] I. P. Grant and B. J. McKenzie, J. Phys. B **13**, 2671 (1980).
- [35] H. M. Quiney, in *Handbook of Molecular Physics and Quantum Chemistry*, Vol. 2, edited by S. Wilson, P. P. Bernath, and R. McWeeny (John Wiley & Sons Ltd., Chichester, 2003) pp. 444–483.
- [36] E. Clementi, *Modern Techniques in Computational Chemistry: MOTECC-91* (ESCOM, 1991).
- [37] F. A. Parpia, A. K. Mohanty, and E. Clementi, J. Phys. B **25**, 1 (1992).
- [38] Y. Ishikawa, H. M. Quiney, and G. L. Malli, Phys. Rev. A **43**, 3270 (1991).
- [39] P. W. Langhoff and M. Karplus, J. Opt. Soc. Am. **59**, 863 (1969).
- [40] R. H. Orcutt and R. H. Cole, J. Chem. Phys. **46**, 697 (1967).
- [41] S. Chattopadhyay, B. K. Mani, and D. Angom, Phys. Rev. A **86**, 022522 (2012).
- [42] B. K. Mani and D. Angom, Phys. Rev. A **81**, 042514 (2010).